

SIMULATING PATHO-REALISTIC ULTRASOUND IMAGES USING DEEP GENERATIVE NETWORKS WITH ADVERSARIAL LEARNING

Francis Tom, Debdoot Sheet

Indian Institute of Technology Kharagpur, India

ABSTRACT

Ultrasound imaging makes use of backscattering of waves during their interaction with scatterers present in biological tissues. Simulation of synthetic ultrasound images is a challenging problem on account of inability to completely model various factors of which some include intra-/inter scanline interference, transducer to surface coupling, artifacts on transducer elements, inhomogeneous shadowing and nonlinear attenuation. While various approaches to ultrasound simulation has been developed, approaches that produce patho-realistic images typically solve wave space equations making it computationally expensive and slow to operate. We propose a generative adversarial network (GAN) inspired approach for fast simulation of patho-realistic ultrasound images. We apply the framework to intravascular ultrasound (IVUS) simulation. A stage 0 simulation is done from the echogenicity map of the tissue obtained from the ground truth label of ultrasound image using an off the shelf pseudo B-mode ultrasound image simulator. The images obtained are adversarially refined using stacked GAN. The stage I GAN generates low resolution images from the images generated by the initial simulation. The stage II GAN further refines the output of the stage I GAN and generates high resolution images which are patho-realistic. We demonstrate that the network generates realistic appearing images evaluated with a visual Turing test indicating an equivocal confusion in discriminating simulated from real. We also quantify the shift in tissue specific intensity distributions of the real and simulated images to prove their similarity.

Index Terms— Adversarial learning, deep convolutional neural network, generative adversarial network, intravascular ultrasound, ultrasound simulation.

1. INTRODUCTION

Fast simulation of realistic ultrasound images is a challenging research problem. Ultrasound images are formed by reflection of ultrasound waves off body structures. Therefore, it takes time for realistic medical ultrasound image simulation as acoustic properties should be incorporated into the simulator for realistic simulation. A simulator that generates realistic images could be used for the generation of large number of

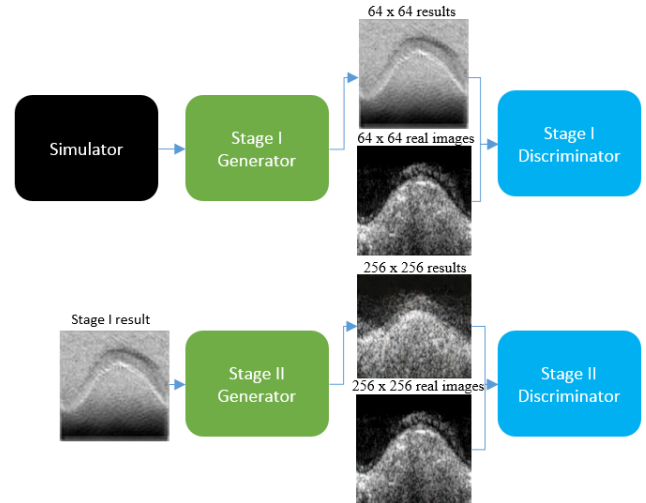


Fig. 1: Overview of the proposed framework for ultrasound simulation using stacked generative adversarial networks.

simulated images which could be used for training supervised machine learning algorithms where the major bottleneck is the sparsity of data. The annotation of the simulated images is a comparatively trivial task. The simulator could also be used as a learning aid for doctors. A large variety of pathologies could be generated by the simulator, which may not be present in case limited real data is available. Fig. 1 summarizes the contribution of this paper where we present a generative adversarial network (GAN) based framework for fast and realistic simulation of ultrasound images.

The rest of the paper is organized as follows: Sec. 2 describes the prior art in ultrasound simulation. Sec. 3 describes our methodology. Sec. 4 presents the results of our experiments on the publicly available border detection in IVUS challenge¹ dataset along with discussion. Sec. 5 presents the conclusions of the work.

2. PRIOR ART

Several approaches have been proposed for the simulation of ultrasound images. In [1], an ultrasonic B-scanning computer

¹<http://www.cvc.uab.es/IVUSchallenge2011/dataset.html>

simulation method was developed with the assumption of linearity, separability and space invariance of the point spread function (PSF) of the imaging system. In [2] a fast GPU-based method using a ray-based model was employed for simulation from volumetric CT scans. In [3], the Born approximation and a scatterer model were used and in [4] a ray-tracing algorithm on histopathology was employed for simulation. Further in [5] the Rayleigh scattering model, physical reflection, transmission and absorption are included to realize a real-time simulation. In [6], the Field II simulator² was combined with a finite element model. In [7], cellular nuclei patterns were used to define ultrasonic scatterers for IVUS simulation. In [8], realistic IVUS simulation was performed from histology images by solving the wave propagation modeled through the Westervelt equation using the finite difference method.

3. METHODOLOGY

Our framework employs (1) Simulation of ultrasound images from the tissue echogenicity maps obtained from the ground truth segmentation labels. (2) Generation of low resolution images from the simulated images using Simulated + Unsupervised learning by Stage I GAN. (3) Generation of high resolution patho-realistic images from the low resolution Stage I images by Stage II GAN.

3.1. Stage 0 simulation from tissue echogenicity map

The ground truth label of lumen and external elastic lamina boundary contour is used to generate the tissue echogenicity map. The initial simulation is performed by a pseudo B-mode ultrasound image simulator³ [1, 9] that assumes a linear and space invariant point spread function (PSF). Image is formed with assumption of wave propagating vertically along the echogenicity map. The images are generated in the polar domain.

$$V(x, y) = h(x, y) * T(x, y) \quad (1)$$

where $V(x, y)$ represents a 2-D ultrasonic data set, where x and y denote axial and lateral coordinates, $T(x, y)$ the raw RF data and $h(x, y)$ the point spread function of the imaging system.

3.2. Stage I GAN

The GAN [10] framework consists of a generator and a discriminator competing against each other to minimize losses that are complementary. The GAN training procedure is a two player minimax game. The generator attempts to generate the

true data distribution while the discriminator attempts to differentiate between true data and the data generated by the generator. Here, refinement of the output of the pseudo B-mode simulator is performed by a two stage stacked GAN [11].

The Stage I GAN is trained to generate a low resolution (64×64) image in the polar domain using the simulated + unsupervised learning approach [12]. This involves learning of a refiner network $G_I(\mathbf{x})$ that refines an image from the pseudo B-mode simulator \mathbf{x} , with θ as the function parameters. The discriminator network ($D_{I\phi}$) is trained to classify whether the images are real or refined, where ϕ denotes the discriminator network's parameters. The refined image is denoted as $\tilde{\mathbf{x}}$. The set of real images $\mathbf{y}_i \in \Upsilon$ are used for learning the parameters. The loss function consists of a realism loss term (l_{real}) and an adversarial loss term. The realism loss term ensures that the ground truth label remains intact in the low resolution refined image which is used to condition the Stage II GAN. During training of the Stage I GAN, the discriminator loss (L_{D_I}) and generator loss (L_{G_I}) are minimized alternately where,

$$L_{G_I}(\theta) = - \sum_j \log(1 - D_{I\phi}(G_{I\theta}(\mathbf{x}_i))) + \lambda l_{reg}(\theta; \mathbf{x}_i) \quad (2)$$

$$L_{D_I}(\phi) = - \sum_i \log(D_{I\phi}(G_{I\theta}(\mathbf{x}_i))) - \sum_j \log(1 - D_{I\phi}(\mathbf{y}_j)) \quad (3)$$

Self-regularization here minimizes per-pixel difference between the refined image and the synthetic image. Therefore,

$$l_{real}(\theta; \mathbf{x}_i) = \|\tilde{\mathbf{x}} - \mathbf{x}\|_1 \quad (4)$$

A buffer of refined images generated over the previous steps was used to improve the realism of the artifacts in the refined images as in [12].

Model architecture: The Stage I GAN generator is a residual network [13] with 4 residual blocks. The simulated image from the pseudo B-mode simulator of size 64×64 is first passed through a convolution layer with 3×3 kernel and a 64 feature map output. The refined image is generated by a convolution layer with 1×1 kernel size. The discriminator network comprises of 5 convolution layers and 2 max pooling layers as in [12].

3.3. Stage II GAN

The generator of the Stage II GAN accepts the low resolution images from the Stage I GAN generator and generates high resolution images adding realistic artifacts. While training the Stage II GAN, the discriminator loss $L_{D_{II}}$ and generator loss $L_{G_{II}}$ are minimized alternately where,

²<http://field-ii.dk/>

³<https://in.mathworks.com/matlabcentral/fileexchange/34199>

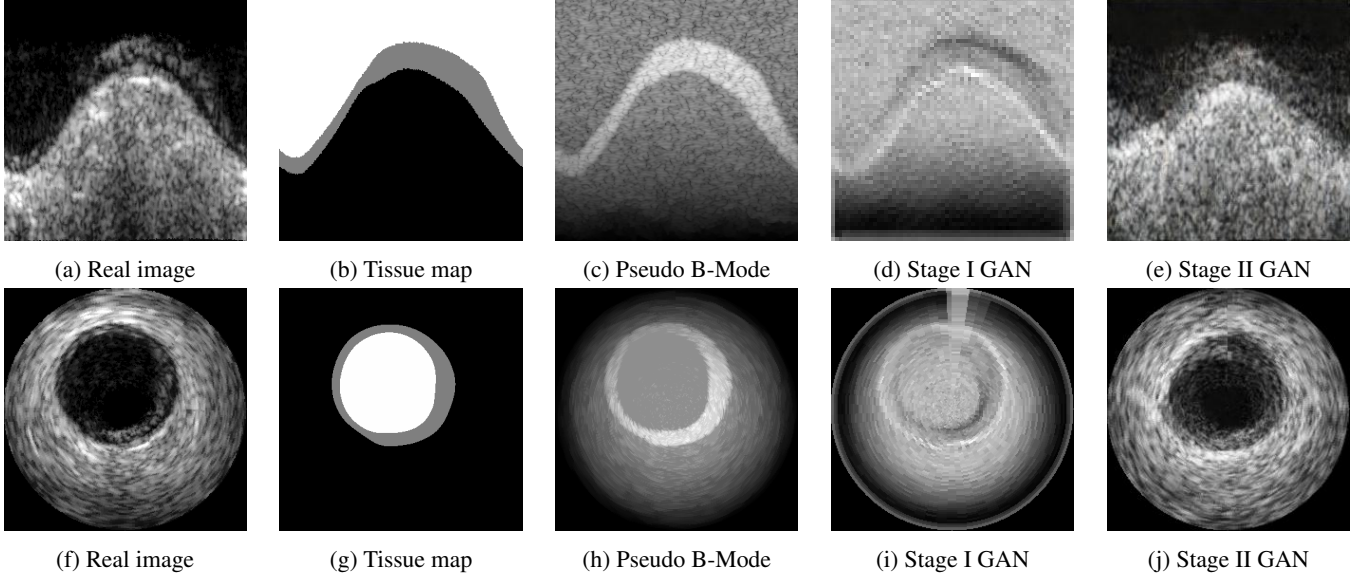


Fig. 2: Comparison of images obtained at different stages of the proposed framework. The first row displays images in the Polar domain and the second row displays the corresponding figures in the Cartesian domain.

$$L_{G_{II}}(\theta) = - \sum_j \log(1 - D_{II\phi}(G_{II\theta}(G_I(\mathbf{x}_i)))) \quad (5)$$

$$L_{D_{II}}(\phi) = - \sum_i \log(D_{II\phi}(G_{II\theta}(G_I(\mathbf{x}_i)))) - \sum_j \log(1 - D_{II\phi}(\mathbf{y}_j)) \quad (6)$$

The high resolution images generated are in polar domain and scan converted to cartesian coordinate domain for visual inspection.

Model architecture: The Stage II GAN generator consists of a downsampling block that comprises of two max-pooling layers to downsample the 64×64 image by a factor of four. The feature maps are then fed to residual blocks, following which upsampling layers upsample the image to 256×256 . The discriminator network consists of downsampling blocks that reduce the dimension to 4×4 followed by a 1×1 convolution layer and a fully connected layer to generate the prediction.

4. EXPERIMENTS, RESULTS AND DISCUSSION

In this section, experimental validation of our proposed framework is presented. Images from the dataset released as part of the border detection in IVUS challenge⁴ was used

⁴<http://www.cvc.uab.es/IVUSChallenge2011/dataset.html>

in our work. The images were obtained from clinical recordings from a 20 MHz probe. Of the 2,175 available images, 435 had been manually annotated. We used 2,025 real images for training (Patient ID 1-9) and 150 images were held out for testing (Patient ID 10). The ground truth label dataset containing 435 images were augmented by rotating each image by 30° over 12 steps. Each such image was then warped by translating up and down by 2% in the polar domain to yield an augmented dataset of 15,660 tissue maps to be processed with the pseudo B-mode simulator.

The Stage I GAN was trained with a learning rate of 0.001 with the Adam optimizer over 20 epochs with a batch size of 512. While training the Stage II GAN, the weights of Stage I GAN were held fixed. Training was done with the Adam optimizer with an initial learning rate of 0.0002, and a learning rate decay of 0.5 per 100 epochs over 1,200 epochs with a batch size of 64.

4.1. Qualitative evaluation of the refined images

In order to evaluate the visual quality of the adversarially refined images, we conduct a Visual Turing Test (VTT). A randomly selected set of 20 pairs of images, with each pair consisting of a real and an adversarially refined image in random order was presented to 13 subjects with experience in clinical or research ultrasonography. They were asked to label the image that appears to be an IVUS in each pair. The subjects correctly identified the real IVUS 147 out of 260 times with 56% chance of correct identification.

Table 1: Quantitative evaluation of divergence between speckle distribution of different regions as compared to the original IVUS.

JS divergence	lumen	media	externa
Stage II GAN	0.0458	0.1159	0.3343
Stage 0	0.0957	0.5245	0.6685

Table 2: Intra tissue variability of speckle distribution between pair of regions in real and refined IVUS images

JS divergence	lumen-media	media-ext.	lumen-ext.
Real	0.2843	0.1460	0.2601
Refined	0.1471	0.1413	0.3394

4.2. Quantitative evaluation of the refined images

In addition to the VTT, we also evaluate the quality of the refined images quantitatively. The histograms of the real and adversarially refined images in the three regions (lumen, media and externa) for 30 randomly chosen annotated images were obtained and the probability mass functions were computed from the histograms. A random walk based segmentation algorithm [14] was used for the annotation of the refined images. The Jensen-Shannon (JS) divergence between the probability mass functions of the lumen, media and the external elastic laminae was computed. The results are summarized in Table 1. The pairwise JS-divergence between lumen and media, media and externa and lumen and externa were computed for both the set of annotated images in the test set and the corresponding adversarially refined images. The results are summarized in Table 2. It is observed that the adversarially refined images are closer to the real images than the images generated by the pseudo B-mode simulator. Thus, adversarial refinement produces images with patho-realistic details.

5. CONCLUSION

Here we have proposed a stacked GAN based framework for the fast simulation of patho-realistic ultrasound images using a two stage GAN architecture to refine images synthesized from an initial simulation performed with a pseudo B-model ultrasound image generator. The quality of the simulated images was evaluated through a visual Turing test to evoke equivocal visual response across experienced raters with 50% chance of identifying the real from simulated IVUS. The quality of the simulated images was quantitatively evaluated using JS divergence between the distributions of the real and simulated images. Similarity of the real and refined images is also quantified by computing the shift in tissue specific speckle intensity distributions. Conclusively these evaluations substantiate ability of our approach to generate patho-realistic IVUS images, converging closer to real ap-

pearance as compared to prior-art, while simulating an image in under 10 ms during deployment.

6. REFERENCES

- [1] J. C. Bamber and R. J. Dickinson, "Ultrasonic b-scanning: a computer simulation," *Phys., Med., Biol.*, vol. 25, no. 3, pp. 463, 1980.
- [2] O. Kutter, R. Shams, and N. Navab, "Visualization and gpu-accelerated simulation of medical ultrasound from ct images," *Comp. Methods, Prog., Biomed.*, vol. 94, no. 3, pp. 250–266, 2009.
- [3] M. D. R. Ramírez, P. R. Ivanova, J. Mauri, and O. Pujol, "Simulation model of intravascular ultrasound images," in *Int. Conf. Med. Image Comput., Comp.-Assist. Interv.*, 2004, pp. 200–207.
- [4] S. C. Groot, R. Hamers, F. H. Post, C. P. Botha, and N. Bruining, "Ivus simulation based on histopathology," in *Proc. Int. Conf. Comp. Cardiol.*, 2006, pp. 681–684.
- [5] C. Abkai, N. Becherer, J. Hesser, and R. Manner, "Real-time simulator for intravascular ultrasound (ivus)," in *Proc. SPIE Med. Imaging*, 2007, vol. 6513, pp. 65131E–1–6.
- [6] F. M. Cardoso, M. C. Moraes, and S. S. Furuie, "Realistic ivus image generation in different intraluminal pressures," *Ultrasound, Med., Biol.*, vol. 38, no. 12, pp. 2104–2119, 2012.
- [7] S. Kraft, A. Karamalis, D. Sheet, E. Drecoll, E. J. Rummeny, N. Navab, P. B. Noël, and A. Katouzian, "Introducing nuclei scatterer patterns into histology based intravascular ultrasound simulation framework," in *Proc. SPIE Med. Imaging*, 2013, vol. 8675, pp. 86750Y–6.
- [8] S. Kraft, S. Conjeti, P. B. Noël, S. Carlier, N. Navab, and A. Katouzian, "Full-wave intravascular ultrasound simulation from histology," in *Int. Conf. Med. Image Comput., Comp.-Assist. Interv.*, 2014, pp. 627–634.
- [9] Y. Yu and S. T. Acton, "Speckle reducing anisotropic diffusion," *IEEE Trans. Image Process.*, vol. 11, no. 11, pp. 1260–1270, 2002.
- [10] I. Goodfellow, J. Pouget-Abadie, M. Mirza, B. Xu, D. Warde-Farley, S. Ozair, A. Courville, and Y. Bengio, "Generative adversarial nets," in *Proc. Adv. Neur. Inf. Process. Sys.*, 2014, pp. 2672–2680.
- [11] H. Zhang, T. Xu, H. Li, S. Zhang, X. Huang, X. Wang, and D. Metaxas, "Stackgan: Text to photo-realistic image synthesis with stacked generative adversarial networks," *arXiv preprint arXiv:1612.03242*, 2016.
- [12] A. Shrivastava, T. Pfister, O. Tuzel, J. Susskind, W. Wang, and R. Webb, "Learning from simulated and unsupervised images through adversarial training," *Proc. IEEE/CVF Conf. Comp. Vis., Patt. Recog.*, pp. 2107–2116.
- [13] K. He, X. Zhang, S. Ren, and J. Sun, "Deep residual learning for image recognition," in *Proc. IEEE/CVF Conf. Comp. Vis., Patt. Recog.*, 2016, pp. 770–778.
- [14] L. Grady, "Random walks for image segmentation," *IEEE Trans. Patt. Anal., Mac. Intell.*, vol. 28, no. 11, pp. 1768–1783, 2006.